RSC Advances

ROYAL SOCIETY OF CHEMISTRY

www.rsc.org/advances

Preparation and performance studies of Polysulfone-Sulfated nano-Titania (S-TiO_2) nanofiltration membranes for dye removal

Valeen Rashmi Pereira[a], Arun M Isloor[a]*, Udaya Bhat K[b], A.F. Ismail[c], Abdulrahman Obaid[d] and Hoong-Kun Fun[d,e]

[a]*Membrane Technology Laboratory, Chemistry Department, National Institute of Technology Karnataka, Surathkal, Mangalore 575 025, India*

[b]*Department of Materials and Metallurgical engineering, National Institute of Technology Karnataka, Surathkal, Mangalore 575 025, India*

[c]*Advanced Membrane Technology Research Center (AMTEC), Universiti Teknologi Malaysia, 81310 Skudai, Johor Bahru, MALAYSIA*

[c]*Department of Pharmaceutical Chemistry, College of Pharmacy, King Saud University, P.O. Box. 2457 - Riyadh 11451, Kingdom of Saudi Arabia.*

[d]*X-ray Crystallography Unit, School of Physics, Universiti Sains Malaysia, Penang 11800, Malaysia.*

Abstract

Polysulfone nanofiltration membranes containing sulfated nano-Titania (S-TiO_2) were fabricated, aiming to enhance the membrane properties along with the possible rejection of Methylene Blue (MB) dye by membranes. Initially S-TiO_2 was synthesized from nano TiO_2 by the action of sulfuric acid. The synthesized S-TiO_2 was characterized by Fourier Transform Infrared spectroscopy (FT-IR), Energy Dispersive Spectrophotometer (EDS) and Transmission Electron Microscope (TEM) analysis. S-TiO_2 was added in increasing concentration into the membranes and their effect on the performance of the membranes was evaluated. The synthesized membranes were characterized by Scanning Electron Microscopy (SEM), Atomic Force Microscopy (AFM). Polysulfone membranes containing S-TiO_2 showed enhancement in properties in terms of hydrophilicity, water uptake, mechanical strength, improved pure water flux (PWF), antifouling nature and high Flux Recovery Ratio (FRR). The polysulfone membranes with S-TiO_2 showed 99 % rejection for BSA (Bovine Serum Albumin) protein molecules during BSA filtration. The prepared membranes were used for the removal of MB dye from aqueous solutions. A maximum of 90.4 % rejection was obtained for MB by the membrane having 2.0 wt. % of S-TiO_2 under UV light radiation. This approach showed that, Polysulfone-

S-TiO_2 membranes displayed good efficiency for dye removal and can be effectively used for the removal of MB dye from aqueous solutions under suitable conditions.

Keywords: Polysulfone, S-TiO_2, BSA, Methylene Blue

Author for correspondence: E-mail address: isloor@yahoo.com, Fax: 91 824 2474033

1. Introduction

Membrane technology has been an important tool in water treatment because of its selective and efficient separation, stability, ease in operation, flexible to be integrated with other separation processes.[1-4] Polysulfone (Psf) is one of the widely used polymers in membrane science owing to its excellent film forming ability and also because of its advantages such as good chemical resistance, mechanical strength, and thermal stability.[5] However polysulfone membranes due to their inherent hydrophobic nature are prone to fouling.[6] This results in adsorption or deposition of foulants on the surface of the membrane and within the membrane pores, leading to decline in permeation flux over a period of time.[7] The hydrophobic interactions between the membrane surface and the solute particles in the feed contribute towards fouling.[8]

A variety of techniques and methods have been developed to modify polysulfone membranes in order to improve its hydrophilicity. Some of them include, blending with hydrophilic polymers, modification of Psf with hydrophilic groups, graft polymerization, plasma treatment, UV-assisted polymerization.[7,8] In the recent years, modification of the membranes by blending with inorganic materials such as nanoparticles has been of great interest because of facile preparation, good dispersion, effective hydrophilicity.[7,9] Among the various nanomaterials, TiO_2 is one of the extensively used nanomaterial in preparing nanocomposite membranes.[10] This is because, TiO_2 nanoparticles provide hydrophilicity, have stability and can also act as photocatalyst in hybrid photocatalyst-membrane based waste water treatment.[11,12] TiO_2 is known to have photocatalytic activity. Focus has been laid on improving its photocatalytic efficiency. One among the efforts is sulfation of TiO_2, where the presence of SO_4^{2-} increases the light absorption and the photocatalytic activity. SO_4^{2-}-TiO_2 has also been used as photocatalyst for the degradation of Methylene Blue (MB) dye.

MB is a cationic dye which has wide applications in textile industry, for coloring paper, dyeing cotton, wool, as hair colorant etc.[13] However, acute exposure to MB can cause health hazards such as increased heart rate, vomiting, cyanosis, tissue necrosis.[14] Also effluents containing dye such as MB is a major toxic industrial waste.[15,16] MB containing waste water stream are highly colored, cause water pollution and are also hazardous to aquatic organisms.[15,17] Hence the colored water needs to be treated and removed before its disposal.[17]

In our present approach, sulfated TiO_2 nanoparticles (S-TiO_2) were synthesized and were used as additives into Psf membranes. S-TiO_2 was added in increasing concentrations into the Psf membranes. The effect of addition of S-TiO_2 on the performance of Psf membranes was analyzed. The membranes containing sulfated nano TiO_2 were used for the removal of Methylene Blue (MB) dye. The MB dye removal with respect to the concentration of S-TiO_2 in the membranes, with and without UV radiation was investigated.

2. Experimental

2.1 Materials

Polysulfone (Psf) having molecular weight of 35,000 Da and TiO_2 nanoparticles were purchased from Sigma Aldrich Co. Bangalore, India. Bovine Serum Albumin (BSA) was obtained from Central Drug House (CDH), New Delhi. Isopropanol and N-methyl-2- pyrrolidone (NMP) was purchased from Merck India, Ltd. Sulphuric acid (H_2SO_4) was purchased from Nice Chemicals Pvt. Ltd., India. Methylene Blue (MB) was purchased from Sigma Aldrich Co. Bangalore, India.

2.2 Preparation of sulfated TiO_2

Sulfated-TiO_2 was synthesized as per the reported literature.[18] TiO_2 nanopowder was dispersed in 50 mL of isopropanol. 2 mL of 1M H_2SO_4 was added to the solution drop wise under stirring. The solution was kept under stirring for about 4 h. The resulting suspension was centrifuged, washed and dried in oven at 100^oC for 24 h. The dry sample was calcined for 5 h at 500^oC.

2.2.1 Characterization of S-TiO_2

Fourier Transform Infrared FTIR spectrometer (SHIMADZU) was used to obtain the IR spectra of TiO_2 and S-TiO_2. Elemental analysis of sulfated samples was carried out with the help

of Energy Dispersive Spectrophotometer (EDS)-(JEOL JSM-6380LA). Transmission electron microscope (TEM)-(JEOL JEM-2100) was used to observe the morphology of sulfated TiO_2.

2.3 Preparation of membranes

Membranes were prepared by phase inversion technique. 20 wt. % of Psf was dissolved in NMP by stirring at 60°C for 24 h to get a homogenous mixture. S-TiO_2 was added to the solution and sonicated for 5 minutes to avoid agglomeration. The solution was further stirred for 1 h. Then the solution was sonicated for 15 min for degassing i.e. to remove any trapped air bubbles. The solution was then left still under heating for 30 min. Finally the solution was casted on the glass plate using Doctor's blade and immersed in distilled water for 24 h for phase inversion. The prepared membranes were then washed thoroughly and air dried. Membranes were prepared with different concentrations of S-TiO_2, whereas the concentration of Psf was fixed to 20 wt. % for all the membranes. The concentration of S-TiO_2 in the membranes was varied as 0 wt. %, 0.05 wt. %, 0.5 wt. %, 1.0 wt. %, 1.5 wt. % and 2.0 wt. % and the membranes were labeled S-0, S-0.05, S-0.5, S-1.0, S-1.5 and S-2.0 accordingly.

2.3.1 Characterization of membranes

2.3.1.1 Morphology of membranes

The morphology of the synthesized membranes was studied by using the cross sectional images of the membranes. The images were taken through Scanning Electron Microscope (SEM) (JEOL JSM-6380LA). Prior to the SEM analysis, the membrane samples were dipped and fractured in liquid nitrogen and then sputtered with gold for conductivity.

2.3.1.2 Porosity and water uptake of membranes

The porosity (ε) of the membranes was determined by gravimetric method,[19] which gives the equation

$$\varepsilon = \frac{w_1 - w_2}{A \times l \times d_w}$$

where w_1 and w_2 are the weights of the wet and dry membrane samples respectively.'A' is the effective membrane area (m^2), 'l' is the membrane thickness (m), d_w is the water density.

The water uptake study of membranes was done as follows. Membrane samples with 1 cm^2 size were kept immersed in distilled water for 24 h. The wet samples were removed from water and the surface water was blotted. The wet weight of the membranes (W_{wet}) was noted

immediately. The samples were kept in oven for drying at 50°C for few h. The dry weight of membrane samples (W_{dry}) was recorded. From the dry and wet weights of the membranes, the water uptake capacity of the membranes was determined using the formula

$$\% \text{ water uptake} = \left(\frac{W_{wet} - W_{dry}}{W_{wet}} \right) \times 100$$

where W_{wet} and W_{dry} are wet and dry weights of the membrane samples respectively.

2.3.1.3 Mechanical property of membranes

The mechanical properties of the membranes were tested using tensile tester (Model: LRX 2.5KN, LLYOD) at room temperature.[20] Rectangular specimens of length 3 cm and width 1 cm were analysed with gauge length of 30 mm. The testing was done at strain rate of 10 mm/min. Triplicate measurements of the samples were taken and the average values were reported.[21]

2.3.1.4 AFM analysis

The AFM analysis of the membranes were performed using Innova SPM Atomic Force Microscope. The membrane surfaces were imaged using antimony doped silicon cantilever having a force constant in the range of 20-80N/m. Small pieces of dry membrane samples were placed on a metal substrate and were imaged in tapping mode with a scan size of 5μm×5μm.The surface roughness of the membranes was evaluated in terms of average roughness (R_a) and root mean square roughness (R_q).

2.3.1.5 Contact angle of membranes

The contact angle of membranes was measured by sessile droplet method using FTA-200 Dynamic contact angle analyzer. In brief, a water droplet was placed on the flat membrane surface and the contact angle between the water droplet and membrane surface was measured.[22] In order to minimize the experimental error, for each membrane sample the contact angle was measured at three different positions and the mean value was noted.

2.3.1.6 Water Permeability

Water permeability of the membranes was analyzed by measuring the pure water flux (PWF) using dead end filtration cell. An effective membrane area of 5 cm^2 was used for the permeation studies. Before the permeation experiments, the membranes were kept immersed in distilled water for 24 h. The membranes were initially compacted for 1 h at 0.8 MPa. After

compaction, the pressure was reduced to 0.6 MPa TMP (Transmembrane Pressure) and the time dependent pure water flux was measured at intervals of 5 min for each of the membranes. The PWF of the membranes was determined using the equation

$$J_{w1} = \frac{Q}{A\,\Delta t}$$

where J_{w1} is the pure water flux expressed in L/m^{2}h, 'Q'is the quantity of pure water collected (L) in time Δt (h), A is the effective membrane area (m^2).

The pure water flux was also measured by varying the pressure from 0.6 to 1.0 MPa for a fixed interval of time for each membrane.

2.3.1.7 Antifouling ability of membranes

To evaluate the antifouling nature of membranes, BSA was chosen as the model protein. Aqueous solution of BSA was prepared at a concentration of 0.8 g/L. Initially, pure water flux J_{w1} (L/m^{2}h) was measured at 0.6 MPa, TMP. Then the filtration cell was filled with BSA and the flux J_p (L/m^{2}h) was measured. After the BSA filtration, the membranes were thoroughly washed and rinsed with water.[23] Then the BSA solution was removed and the water flux J_{w2} (L/m^{2}h) was measured again under same conditions.[24] The antifouling ability of membranes was evaluated in terms of FRR, given by the formula

$$\text{FRR}\,(\%) = \frac{J_{w2}}{J_{w1}} \times 100$$

The fouling of the membranes was further assessed in terms of total fouling ratio(R_t), reversible fouling (R_r) and irreversible fouling ratio (R_{ir}) which was calculated using the equations[25,26]

$$R_t(\%) = \left(1 - \frac{J_p}{J_{w1}}\right) \times 100$$

$$R_r(\%) = \left(\frac{J_{w2} - J_p}{J_{w1}}\right) \times 100$$

$$R_{ir}(\%) = \left(\frac{J_{w1} - J_{w2}}{J_{w1}}\right) \times 100$$

The % rejection of BSA by the membranes was determined using the equation

$$\%R = \left(1 - \frac{C_p}{C_f}\right) \times 100$$

where C_p (mg/ml) and C_f (mg/ml) are concentrations of BSA in the permeate and the feed respectively.[27]

2.3.1. 8 BSA adsorption Experiment

BSA solution having a concentration of 0.8 g/L was prepared by dissolving BSA.[28] Each membrane having an effective area of 2 cm×2 cm was immersed in 12.0 mL of BSA solution in an air tight bottle for 24h at 28°C.[29] The amount of BSA adsorbed onto the membranes was estimated by calculating the concentration of BSA in the solution, before and after BSA adsorption.

2.3.1.9 Dye Removal by membranes

The dye removal efficiency of membranes was evaluated using Methylene Blue (MB) dye. Aqueous solutions of MB at a concentration of 10 ppm and 20 ppm were prepared. 0.1 g of each of the membrane was weighed and then cut into smaller pieces and were transferred into 6 different conical flasks containing 25 mL of 10 ppm aqueous MB solution. The solutions were shaken continuously at 120 rpm inside an orbital shaker (ORBITEK LT) for 15 hrs under closed/dark conditions. After 15 hrs, aliquots of the suspensions were taken and the concentration of MB dye in the aqueous solutions was analyzed using UV/Vis Spectrophotometer (SPECORD S 600). The experiments were repeated in a similar manner for MB solutions at 20 ppm concentration.

To study the degradation of MB using UV light, a UV source-UV tube (UV-C) of 11W (PHILIPS) was placed 15 cm above the solutions inside the orbital shaker. The experiments were carried out under UV light, in a similar manner as mentioned above, for 15 hrs , for 10 ppm and 20 ppm concentration of MB solutions for each of the membrane samples. The possible damage under UV irradiation to the membrane containing S-TiO_2 was evaluated by observing the surface of the membranes under SEM (Supporting Information-S1). The dye removal by the membranes was evaluated in terms of % rejection, which was calculated using the formula

$$\%\ Rejection = \left(1 - \frac{C_p}{C_f}\right) \times 100$$

Where C_i and C_f are the initial and final concentrations of MB in the aqueous solutions.

3. Results and Discussions

3.1 Characterization of S-TiO_2 nanoparticles

The FT-IR spectra of S-TiO_2 and TiO_2 is shown in Fig. 1. Broad peak around 3200 cm^{-1} and peak at 1642 cm^{-1} is due to the stretching vibrations of surface hydroxyl group and adsorbed water.[23] The peak at 1399 cm^{-1} is due to the stretching frequency of S=O bond and two peaks at 1130 cm^{-1} and 1045 cm^{-1} correspond to the characteristic frequencies of SO_4^{2-}.[18,30] These peaks are not found in TiO_2. Bands in the lower wavelength region ranging from 600-1000cm^{-1} can be ascribed to the Ti-O-Ti vibration.[30]

Figure-1

The EDS spectrum of of S-TiO_2 is given in Fig. 2 which shows the presence of sulfur in the sample.[18] The presence of sulfur in S-TiO_2 was also analysed by elemental mapping of S-TiO_2 (Fig. 3).

Figure-2

Figure-3

Fig. 4 shows the TEM images of TiO_2 and S-TiO_2 nanoparticles. The nanoparticle diameters were found to range from 20 to 30 nm. The morphology of the TiO_2 nanoparticles which is spherical in shape (Fig.4 A) turned to somewhat oval shape after sulfation (Fig. 4 B), which may be due to the result of action of sulfuric acid treatment during sulfation.[18]

Figure-4

3.2 Membrane characteristics

3.2.1 Membrane morphology

The cross sectional images of the membranes are shown in Fig. 5 and Fig. 6. The SEM images display the typical asymmetric structure of membranes having dense top layer, porous sublayer and macrovoids at the bottom. With the addition of S-TiO_2 to the membranes, change in morphology of the membranes is observed.

Figure-5

Figure-6

The porous nature of the membranes was found to increase with the addition of S-TiO_2 and was maximum for S-2.0 membrane whereas, the pristine membrane S-0, which did not contain any S-TiO_2 had very less pores in it. Except for the membranes S-0, S-0.05, the porous

nature was also observed in the skin layer of the membranes. The addition of S-TiO_2 has resulted in imparting significant change to the morphology of the membranes. The addition of S-TiO_2 decreases the thermodynamic stability of the system. This leads to the rapid demixing between the solvent and non solvent which results in enhanced porosity of the membranes.[31,32] It can also be noted that, the macrovoids which were prominent in the pristine, S-0 and S-0.05 membranes, were suppressed and were almost disappearing in the S-1.5, S-2.0 membranes, where the concentration of S-TiO_2 was higher. Similar results were also observed, when TiO_2 was added to the polysulfone membranes.[33]

As observed in SEM images (Fig. 6 E, F), the membranes at higher concentrations, which contained 1.5 and 2.0 wt. % of S-TiO_2, showed the presence of S-TiO_2 in the membrane pores. Also some of the S-TiO_2 nanoparticles at 2.0 wt. %, were found to form large aggregates and hence blocking the pores, as displayed in the magnified image (Fig. 6 F-1) of S-2.0 membrane.

3.2.2 Porosity and Water Uptake of membranes

The porosity and water uptake of the membranes is given in Table 1. It is observed that, the porosity of the membranes increases with the addition of S-TiO_2. The presence of hydrophilic S-TiO_2 would facilitate the formation of pores. Hence as the concentration of S-TiO_2 in the membranes increases, more number of pores would be formed, resulting in higher porosity of the membranes.

The water uptake of the membranes was in the order S-0<S-0.05<S-0.5<S-1.0<S-1.5<S-2.0 (Table 1) i.e., as the concentration of S-TiO_2 in the membranes increased, the water uptake also increased. Water uptake by the membranes depends on membrane porosity. As the porosity of the membranes increases, water uptake ability of the membranes also increases.

Table-1

3.2.3 Mechanical strength analysis

Tensile strength and elongation at break are two important criteria which decides the mechanical stability of the membranes.[34] As seen in Table 2, the tensile strength and elongation at break of the membranes increased with the increase in S-TiO_2, from 12.29 MPa (S-0) to 23.59 MPa (S-2.0) and 111.43 % (S-0) to 123.63 % (S-2.0) respectively. The improvement in mechanical property is due to TiO_2 which is known to have good mechanical stability and also due to the good dispersion of S-TiO_2 in the membrane matrix, which causes strong interaction

between S-TiO_2 and polymer matrix.[35] Also the presence of S-TiO_2 suppresses the formation of macrovoids, thus improving the mechanical properties of the membranes.[34]

Table-2

3.2.4 AFM analysis

The two-dimensional and three dimensional AFM images of the selected membranes, S-0, S-1.0 ans S-2.0 membranes are shown in Fig. 7. The addition of S-TiO_2 into the membranes induced changes on the membrane surface. The neat S-0 membrane which did not contain any S-TiO_2 nanoparticles appeared to be rough whereas the surface roughness was found to decrease with the addition of S-TiO_2. This was confirmed by the surface roughness parameters observed for the membranes (Table 3) which is expressed in terms of mean roughness (R_a) and root mean square roughness (R_q).

Figure-7

Table-3

3.2.5 Contact Angle of membranes

Contact angle is used to determine the hydrophilicity and wetting ability of membrane surface. The contact angle of neat Psf membrane (S-0) was about 70^o, whereas S-TiO_2 containing membranes showed lower contact angle. With the addition of S-TiO_2, the contact angle of the membranes decreased, indicating that the hydrophilicity of the membranes is elevated by the addition of S-TiO_2. The contact angle was least (60^o) for S-1.0 membrane with S-TiO_2 content of 1.0 wt. %, and thereafter for S-1.5 and S-2.0 membranes, the contact angle slightly increased. This may be due to the reason that at 1.5 and 2.0 wt. %, the high content of S-TiO_2 would block the membrane pores, resulting in higher contact angle. However S-1.5 and S-2.0 membranes were more hydrophilic than the neat Psf (S-0) membrane as shown in Fig. 8. Fig. 9 shows the images of the contact angles measured on the membrane surfaces.

Figure-8

Figure-9

3.2.6 Water Permeability of membranes

The time dependent pure water flux of the membranes is shown in Fig. 10. The water permeability of the nanocomposite membranes was superior when compared with the pure Psf membrane. The PWF of the membranes increased with the increase in S-TiO_2 content, especially after 0.05 wt.% of S-TiO_2 content. When the S-TiO_2 content was 2.0 wt.%, the pure water flux reached maximum of about 6.37 $Lm^{-2}h^{-1}$ which is nearly 12 times higher than that of S-0 membrane.[36] The increase in flux is due to the lower membrane resistance offered by the thinner skin layer and higher porosity.[37] The improvement in membrane hydrophilicity with S-TiO_2 will also facilitate the diffusion of water through the membrane.[38] Water flux of the membranes also depends on the morphology of the membranes. As shown in SEM images of the membranes (Fig. 5 and 6), the internal structure of the membranes changed from closed structure to well interconnected pores, resulting in improving the water flux.[9]

The PWF of the membranes vs. pressure is shown in Fig. 11. The pure water flux of all the membranes increased with the increase in applied pressure. This is because, the driving force for the permeation of pure water through membranes is enhanced by the increase in transmembrane pressure.

Figure-10

Figure-11

3.2.7 Antifouling nature of membranes

Fig. 12 shows the time dependent flux behavior of the membranes during BSA filtration along with the water flux before and after the BSA filtration. As observed in Fig. 12, the initial flux for 30 minutes refers to the pure water flux. For next 30 minutes the flux given is with respect to the BSA filtration. The flux of the membranes during BSA filtration was much lower than that of the pure water flux. This is due to the reason that, the BSA molecules present in the feed solution get adsorbed or deposit on the membrane surface resulting in partial blocking of the pores, thus resulting in lower flux.[37,39]

Figure-12

Figure-13

After the BSA filtration, the membranes were washed thoroughly and the water flux was measured again.[40] Here we observe an increase in flux, which implies that BSA molecues were

removed from membrane surface during washing, which results in good flux recovery. Depending on the obtained flux value, FRR value for each of the membranes was calculated in order to evaluate the antifouling ability of the membranes. FRR is the measure of antifouling nature of the membranes. Higher the FRR value, better is the antifouling nature of the membranes. Fig. 13 shows the FRR values of the membranes. FRR value is least for S-0 membrane which is about 76%, whereas for the nanocomposite membranes, FRR increased with the S-TiO_2 content and reached maximum of 93 % for S-2.0 membrane. The presence of sulfated nano TiO_2 weakened the interaction between the membrane surface and BSA molecules. Also high FRR value indicated that, the adsorbed BSA molecules on the membrane surface were removed during hydraulic cleaning. The total fouling of the membranes in terms of total fouling (R_t) along with reversible fouling (R_r) and irreversible fouling (R_{ir}) is shown in Fig. 14. Both R_r and R_{ir} of all nanocomposite membranes were lower than than the pristine polysulfone membranes. The neat polysulfone membrane (S-0) showed highest value of R_t indicating that pristine Psf membranes is more prone to fouling. Both reversible fouling (R_r) and irreversible fouling (R_{ir}) ratios decreases with the increase in S-TiO_2 in the membranes and is least for S-2.0 membrane.

Figure-14

The antifouling nature of the membranes was supported by the AFM results. From AFM measurements it was found that the membranes containing S-TiO_2 nanoparticles were smooth (Fig. 7, Table 3). Lower the surface roughness of the membranes, higher would be the antifouling nature of the membranes.[41]

The BSA rejection % by the membranes is shown in Fig. 15. The rejection properties of all the nanocomposite membranes except neat Psf membrane were almost same. The rejection % of BSA by the neat Psf membrane (S-0) was 88% and the rejection % of all the nanocomposite membranes was 99%. Since the BSA molecules were larger in size than the pore size of the membranes, almost all the BSA molecules were rejected by the membranes.

Figure-15

3.2.8 BSA adsorption by membranes

BSA adsorption study reflects the antifouling nature of the membranes. Lower the amount of BSA adsorbed on the membranes, higher the antifouling nature of the membranes.[29] Fig. 16 shows the BSA adsorption by the membranes. It can be noted that neat Psf S-0 membrane showed highest BSA adsorption, indicating that it is easily fouled by BSA. However all the Psf-S-TiO_2 nanocomposite membranes showed dramatic decrease in protein adsorption. These results are in agreement with the FRR values for the membranes (Fig. 13). Moereover the contact angle measurement also revealed that Psf- S-TiO_2 membranes showed better hydrophilicity which can improve the wettability of the membranes.[29] This can cause the formation of water layer on the membrane surface, which retards the approach of protein molecules, thus improving the membrane resistance to protein deposition, when immersed in aqueous protein solutions.[25,28]

Figure-16

3.2.9 Dye Removal by membranes

Fig. 17 and Fig. 18 shows the MB rejection by the membranes under dark and UV conditions at 10 ppm and 20 ppm MB concentrations respectively. The membranes showed a maximum rejection of 90.4 % at 10 ppm concentration of MB under UV radiation , whereas the neat Psf membranes showed lowest rejection of 13.3 % at 20 ppm of MB concentration.

Figure-17

Figure-18

It can be seen that, the MB rejection increased with the increase in S-TiO_2 content in the membranes and was found to be least for the Psf membranes. The MB dye removal by the membranes takes place by two mechanisms, i.e., by adsorption and photodegradation.[42]

Figure-19

The dye removal by adsorption is as follows. Due to the presence of SO_4^{2-}-TiO_2, the membrane is negatively charged. Since MB is a cationic dye, it can easily get adsorbed on the membrane surface by electrostatic interactions.[43] Hence the retention of MB by the membranes is due to the adsorption of MB on the membrane surface and in the pores.[17] The adsorption of MB on the membrane surface is shown in the Fig. 19 and Fig. 20. It is seen that, the membranes

changed from white to blue when immersed in MB solution and also as the S-TiO_2 content in the membranes increases, the adsorption also increases.[20] This is because, more adsorption sites are available at higher content of S-TiO_2. The adsorption of MB on the membrane surface was confirmed by elemental mapping of Nitrogen (element which is present in MB) as shown in Fig. 21.

Figure-20

Figure-21

Comapring dye rejection in Fig. 17 and Fig. 18, it can be noted that the increase in MB concentration from 10 ppm to 20 ppm results in fall of dye rejection by the membranes. MB being a cationic dye, present in the solution get adsorbed on the membrane surface and neutralize the negative charge present on the membrane surface. Hence the available adsorption sites on the membrane surface for MB becomes gradually less and also the electrostatic force of attraction between the membrane surface and MB is gradually weakened.[42] Hence the possible interaction between MB and membrane surface is reduced at higher concentration of MB. Therefore the rejection of MB by the membranes was low at higher concentration. Fig. 22 shows rejection of MB by the membranes with reference to the color of the solutions.

Figure-22

The dye removal by the membranes by photodecomposition takes place as follows. During the photodecomposition, MB degradation occurs mainly due to the hydroxyl radical ($^{\cdot}OH$). TiO_2 is a photo catalyst, which when photoexcited at a wavelength below 380 nm, the photons excite the electrons (e^-) from valence band to the conduction band, leaving behind the holes (h^+) in the valence band. The holes react with water or hydroxide ions producing hydroxyl radical, which degrade MB.[44] But in TiO_2, photocatalytic activity is limited due to the recombination of electrons and holes resulting in low photo efficiency.[45] In sulfated TiO_2, the presence of SO_4^{2-} improves the photocatalytic efficiency and hence intern increases the MB degradation. The MB rejection by pure S-TiO_2 has also been evaluated (Supporting Information-S2).The sulfation of TiO_2 in S-TiO_2 results in strong acidity giving rise to Lewis acid sites or electron deficient sites. They act as electron trap for photogenerated electron, thereby increasing the life time of $^{\cdot}OH$ radical resulting in enhanced photocatalytic activity.[44,45] Also the acidified

surface in S-TiO_2, on calcination, would lead to the generation of oxygen deficiency, which again serve as capture centers for photoexcited electrons. This hinders the recombination of electrons and holes, while the surrounding hydroxyl groups react with photoexcited holes to generate ·OH radicals, which are the main oxidants in MB degradation.[30,45]

4. Conclusions

Sulfated-TiO_2 (S-TiO_2) can be used as effective additives to Polysulfone (Psf) membranes to improve the properties of membranes in terms of hydrophilicity, porosity, water uptake and water flux. Psf membranes with S-TiO_2 exhibited good antifouling nature. The improvement in properties of Psf membranes depend on the concentration of S-TiO_2 in the membranes. Higher the S-TiO_2 content, better is the performance of the membranes. However at higher concentration i.e. at 1.5 wt.% and 2.0 wt.% of S-TiO_2, aggregation of nanoparticles in the membranes is observed, which may hinder the performance of the membranes to some extent. The synthesized membranes can be used effectively for the removal of BSA molecules, with rejection of 99 %. The prepared membranes have potential in dye removal and can be used for the removal of MB dye from aqueous solutions. The Psf-S-TiO_2 membranes are more effective in MB dye removal under UV irradiation. The MB dye removal by the membranes increased with S-TiO_2 content in the membranes and S-2.0 membrane showed highest rejection of 90.4% at 10 ppm concentration of MB under UV radiation.

Acknowledgements

AMI is thankful to The Director, National Institute of Technology Karnataka, Surathkal, India, for providing the research facilities. The authors also thank Prof. Narayan Prabhu, Department of Metallurgical and Materials Engineering, NITK Surathkal, India, for providing contact angle measurement facilities. The authors extend their appreciation to The Deanship of Scientific Research at King Saud University for funding the work through research group project no. RGP-VPP-207.

References

1. S. Zhao, W. Yan, M. Shi, Z. Wang, J. Wang and S. Wang, *J. Membr. Sci.*, 2015, **478**, 105-116.
2. M. M. Mahlambi, O. T. Mahlangu, G. D. Vilakati and B. B. Mamba, *Ind. Eng. Chem. Res.*, 2014, **53**, 5709-5717.

3. A. Aluigi, F. Rombaldoni, C. Tonetti and L. Jannoke, *J. Hazard. Mater.*, 2014, **268**, 156-165.
4. X. Q. Cheng, L. Shao and C. H. Lau, *J. Membr. Sci.*, 2015, **476**, 95-104.
5. S. Habibi, A. Nematollahzadeh and S. A. Mousavi, *Chem. Eng. J. (Lausanne)*, 2015.
6. M. S. Rahaman, H. Thérien-Aubin, M. Ben-Sasson, C. K. Ober, M. Nielsen and M. Elimelech, *J. Mater. Chem. B*, 2014, **2**, 1724-1732.
7. Y.-F. Zhao, L.-P. Zhu, Z. Yi, B.-K. Zhu and Y.-Y. Xu, *J. Membr. Sci.*, 2013, **440**, 40-47.
8. H. Song, Y. Jo, S.-Y. Kim, J. Lee and C. Kim, *J. Membr. Sci.*, 2014, **466**, 173-182.
9. A. Qin, X. Li, X. Zhao, D. Liu and C. He, *J. Membr. Sci.*, 2015, **480**, 1-10.
10. D. Emadzadeh, W. J. Lau, T. Matsuura, M. Rahbari-Sisakht and A. F. Ismail, *Chem. Eng. J. (Lausanne)*, 2014, **237**, 70-80.
11. N. Hamid, A. F. Ismail, T. Matsuura, A. Zularisam, W. J. Lau, E. Yuliwati and M. S. Abdullah, *Desalination*, 2011, **273**, 85-92.
12. S. Rajesh, S. Senthilkumar, A. Jayalakshmi, M. Nirmala, A. Ismail and D. Mohan, *Colloids Surf., A*, 2013, **418**, 92-104.
13. J.-H. Huang, C.-F. Zhou, G.-M. Zeng, X. Li, J. Niu, H.-J. Huang, L.-J. Shi and S.-B. He, *J. Membr. Sci.*, 2010, **365**, 138-144.
14. P. Mohapatra and K. Parida, *J. Mol. Catal. A: Chem.*, 206, **258**, 118-123.
15. G.-M. Zeng, X. Li, J.-H. Huang, C. Zhang, C.-F. Zhou, J. Niu, L.-J. Shi, S.-B. He and F. Li, *J. Hazard. Mater.*, 2011, **185**, 1304-1310.
16. L. Shao, X. Q. Cheng, Y. Liu, S. Quan, J. Ma, S. Z. Zhao and K. Y. Wang, *J. Membr. Sci.*, 2013, **430**, 96-105.
17. A. B. Fradj, S. B. Hamouda, H. Ouni, R. Lafi, L. Gzara and A. Hafiane, *Sep. Purif. Technol.*, 2014, **133**, 76-81.
18. B. Krishnakumar and M. Swaminathan, *J. Mol. Catal. A: Chem.*, 2011, **350**, 16-25.
19. R. Kumar, A. Ismail, M. Kassim and A. M. Isloor, *Desalination*, 2013, **317**, 108-115.
20. L. Zheng, Y. Su, L. Wang and Z. Jiang, *Sep. Purif. Technol.*, 2009, **68**, 244-249.
21. G. D. Vilakati, E. M. Hoek and B. B. Mamba, *Polym. Test.*, 2014, **34**, 202-210.
22. M. Padaki, A. M. Isloor, G. Belavadi and K. N. Prabhu, *Ind. Eng. Chem. Res.*, 2011, **50**, 6528-6534.
23. V. R. Pereira, A. M. Isloor, A. Al Ahmed and A. Ismail, *New J. Chem.*, 2015, **39**, 703-712.
24. S. Rajesh, A. F. Ismail and D. R. Mohan, *RSC Adv.*, 2012, **2**, 6854-6870.
25. L. Shao, Z. X. Wang, Y. L. Zhang, Z. X. Jiang and Y. Y. Liu, *J. Membr. Sci.*, 2014, **461**, 10-21.
26. S. Shenvi, A. Ismail and A. M. Isloor, *Ind. Eng. Chem. Res.*, 2014, **53**, 13820-13827.
27. V. R. Pereira, A. M. Isloor, U. K. Bhat and A. F. Ismail, *Desalination*, 2014, **351**, 220-227.
28. Z. Yi, L. Zhu, Y. Xu, J. Jiang and B. Zhu, *Ind. Eng. Chem. Res.*, 2011, **50**, 11297-11305.
29. Z.-X. Wang, C.-H. Lau, N.-Q. Zhang, Y.-P. Bai and L. Shao, *J. Mater. Chem. A*, 2015.
30. A. Gambhire, M. Lande, B. Arbad, S. Rathod, R. Gholap and K. Patil, *Mater. Chem. Phys.*, 2011, **125**, 807-812.
31. H. Rabiee, M. H. D. A. Farahani and V. Vatanpour, *J. Membr. Sci.*, 2014, **472**, 185-193.
32. G. Zhang, S. Lu, L. Zhang, Q. Meng, C. Shen and J. Zhang, *J. Membr. Sci.*, 2013, **436**, 163-173.
33. Y. Yang, H. Zhang, P. Wang, Q. Zheng and J. Li, *J. Membr. Sci.*, 2007, **288**, 231-238.
34. F. Shi, Y. Ma, J. Ma, P. Wang and W. Sun, *J. Membr. Sci.*, 2012, **389**, 522-531.
35. A. Abdal-hay, H. M. Mousa, A. Khan, P. Vanegas and J. H. Lim, *Colloids Surf., A*, 2014, **457**, 275-281.
36. J. Zhang, Y. Zhang, Y. Chen, L. Du, B. Zhang, H. Zhang, J. Liu and K. Wang, *Ind. Eng. Chem. Res.*, 2012, **51**, 3081-3090.
37. J. Peng, Y. Su, W. Chen, Q. Shi and Z. Jiang, *Ind. Eng. Chem. Res.*, 2010, **49**, 4858-4864.
38. H. Huang, X. Qu, X. Ji, X. Gao, L. Zhang, H. Chen and L. Hou, *J. Mater. Chem. A*, 2013, **1**, 11343-11349.
39. R. Kumar, A. M. Isloor, A. F. Ismail, S. A. Rashid and T. Matsuura, *RSC Adv.*, 2013, **3**, 7855.

40. Y.-F. Zhao, P.-B. Zhang, J. Sun, C.-J. Liu, Z. Yi, L.-P. Zhu and Y.-Y. Xu, *J. Colloid Interface Sci.*, 2015.
41. A. Razmjou, J. Mansouri and V. Chen, *J. Membr. Sci.*, 2011, **378**, 73-84.
42. S. Mozia, M. Toyoda, T. Tsumura, M. Inagaki and A. W. Morawski, *Desalination*, 2007, **212**, 141-151.
43. H. Li, Y. Lin, Y. Luo, P. Yu and L. Hou, *J. Hazard. Mater.*, 2011, **192**, 490-499.
44. M. M. Mohamed and M. M. Al-Esaimi, *J. Mol. Catal. A: Chem.*, 2006, **255**, 53-61.
45. C. Zhan, F. Chen, J. Yang, D. Dai, X. Cao and M. Zhong, *J. Hazard. Mater.*, 2014, **267**, 88-97.

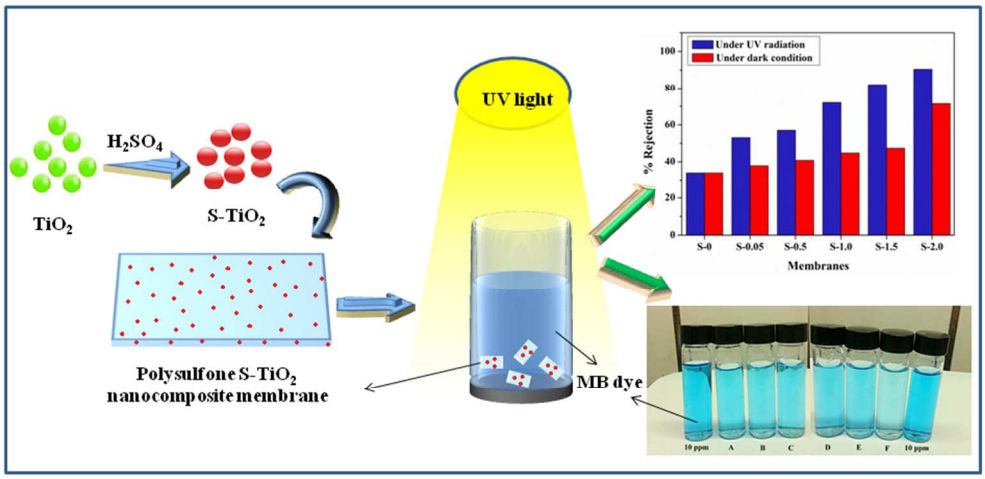

81x40mm (300 x 300 DPI)

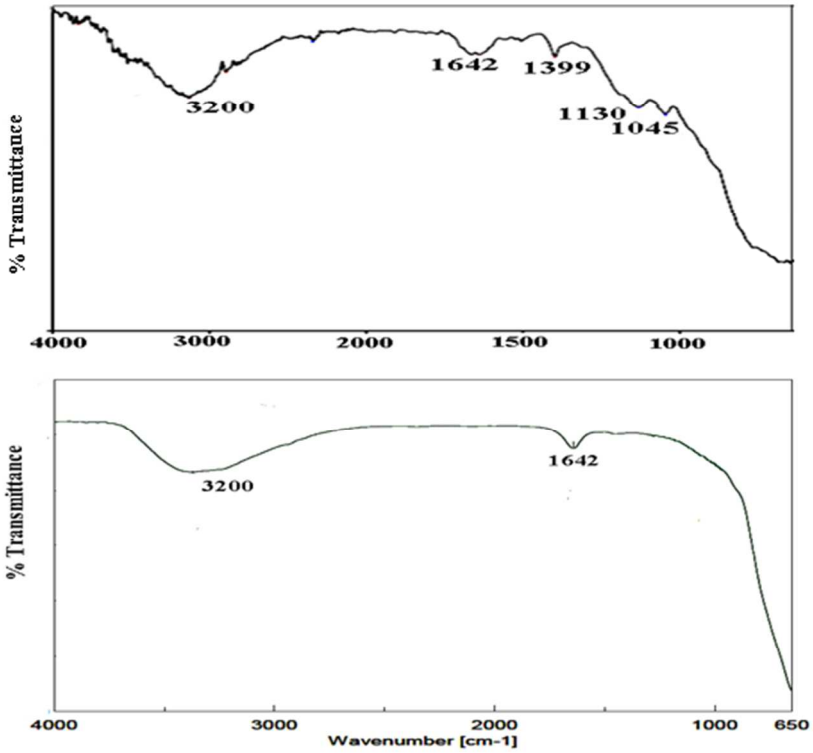

Fig. 1 FT-IR spectra of S-TiO_2 and TiO_2 .

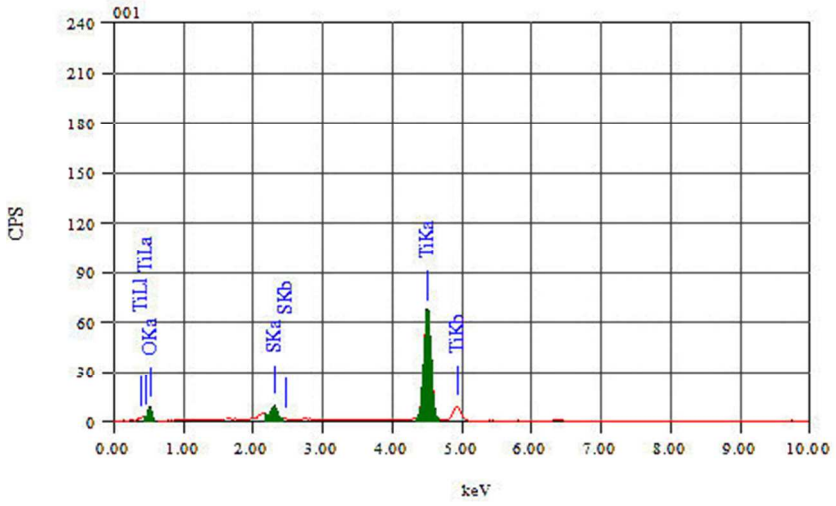

Fig. 2 EDS spectrum of S-TiO_2.

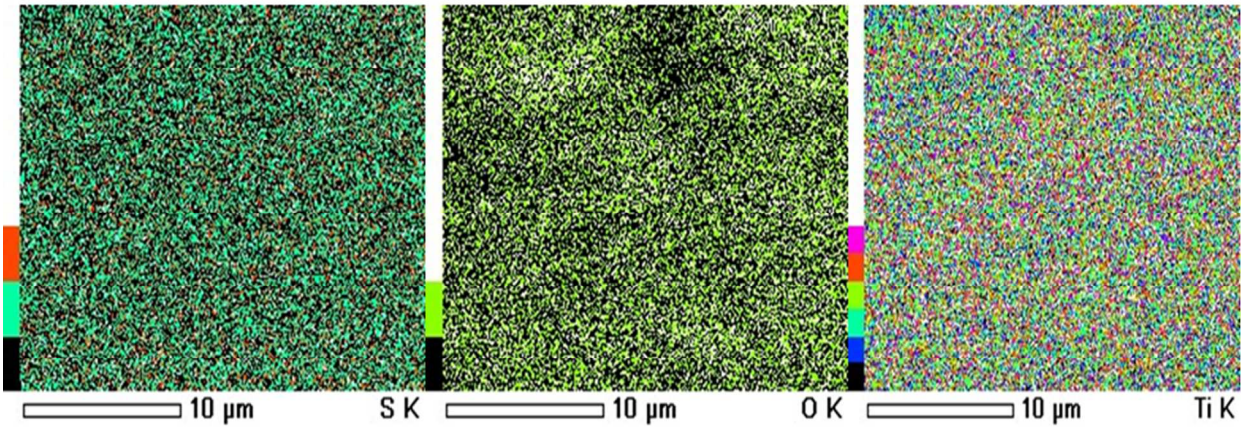

Fig. 3 Elemental mapping of S-TiO_2 showing the presence of Sulfur(S), Oxygen(O) and Titanium (Ti) in the sample.

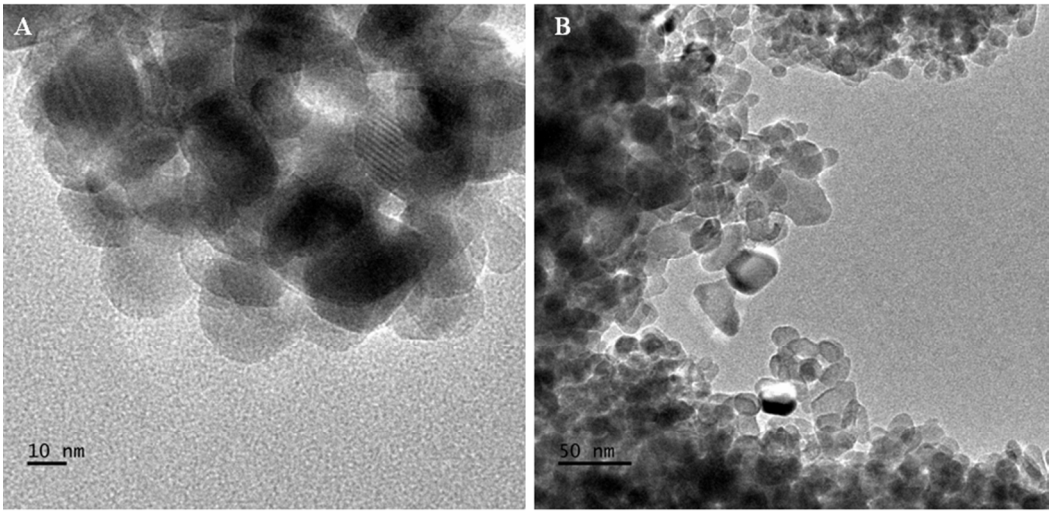

Fig. 4 TEM Images of A) TiO_2 and B) S-TiO_2.

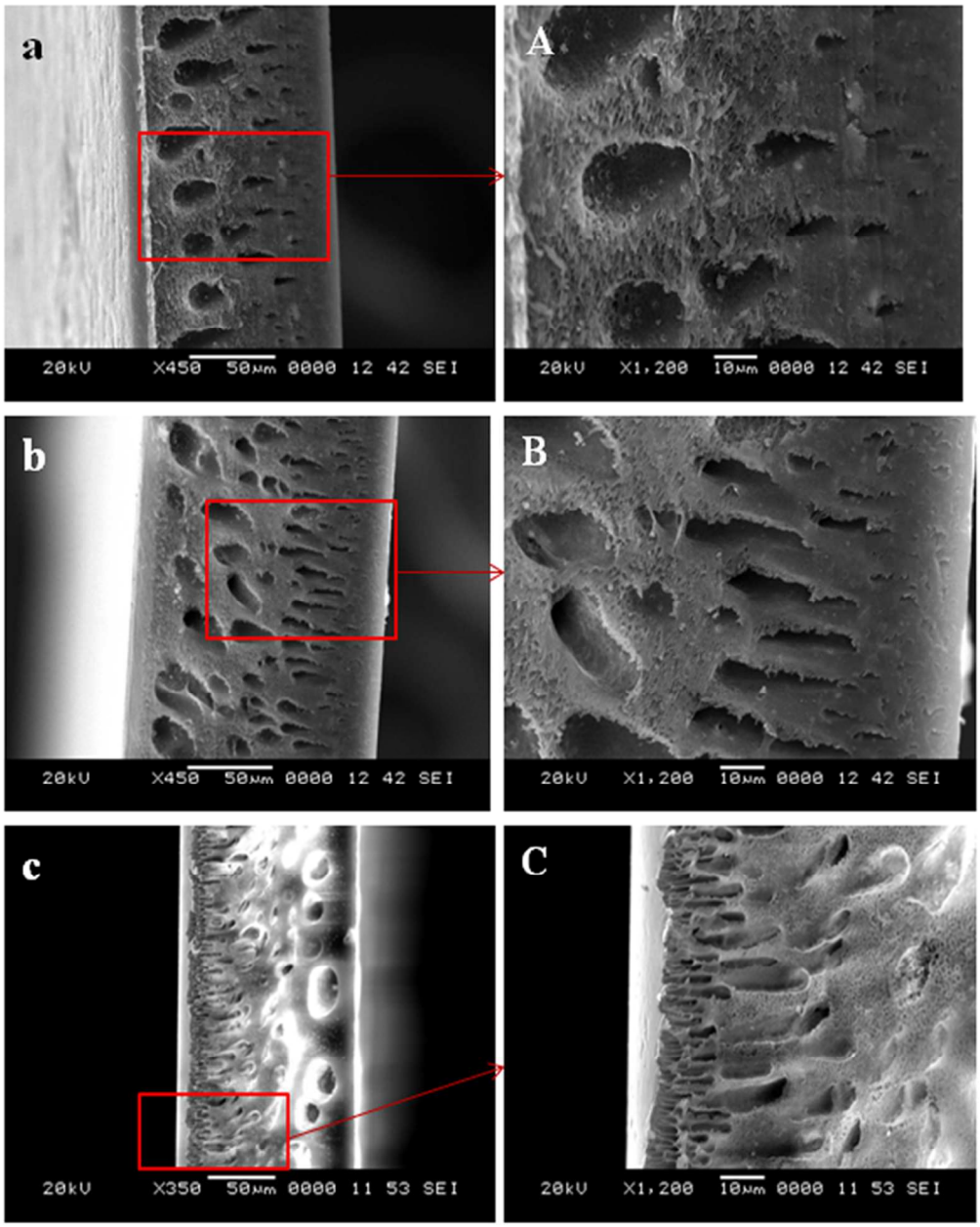

Fig. 5 SEM cross sectional images of membranes a)S-0 b)S-0.05 c) S-0.5 (A, B, C are magnified images of a, b, c respectively).

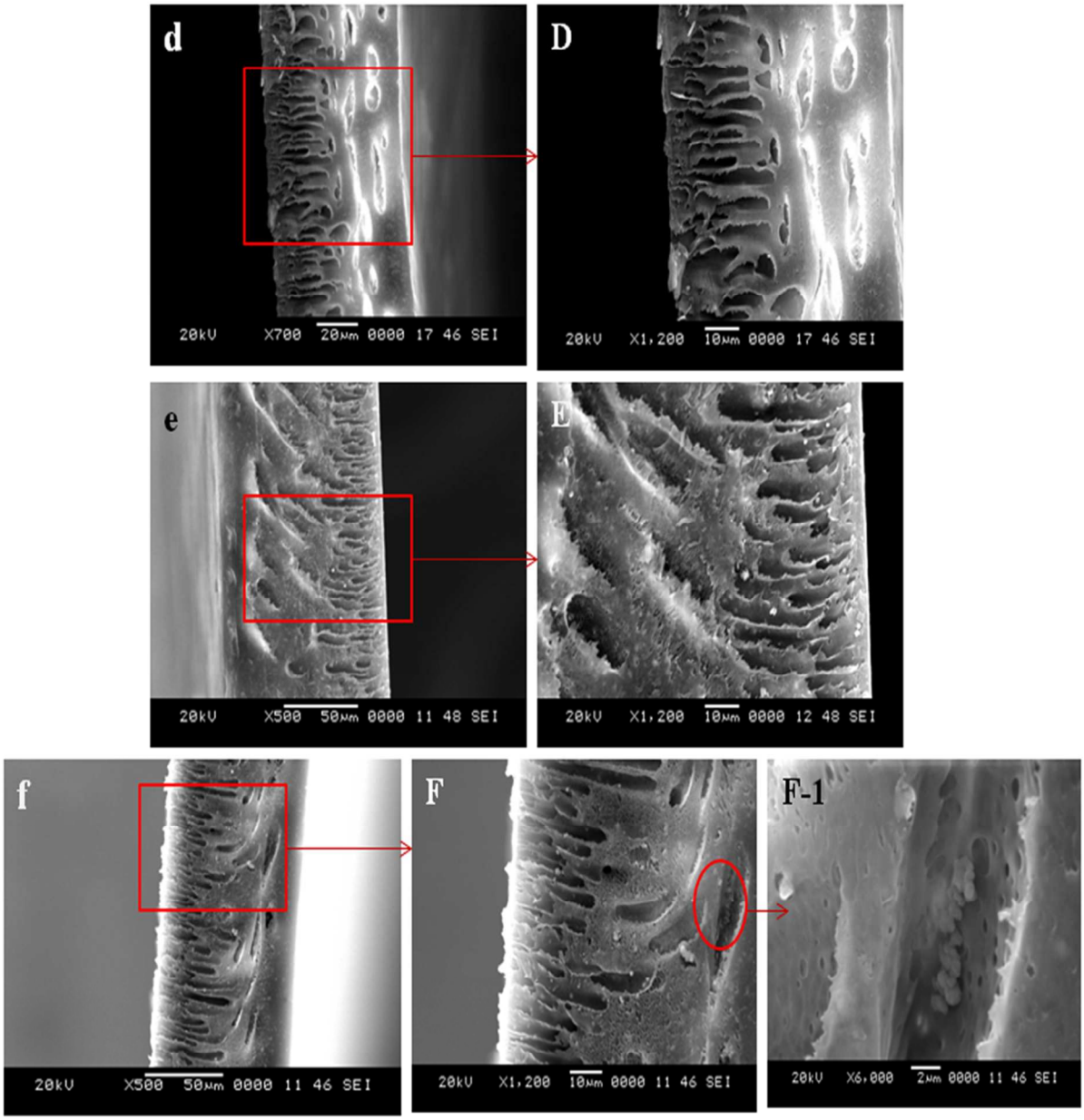

Fig. 6 SEM cross sectional images of membranes d) S-1.0 e) S-1.5 f) S-2.0 (D, E, F are the magnified images of d, e, f respectively).

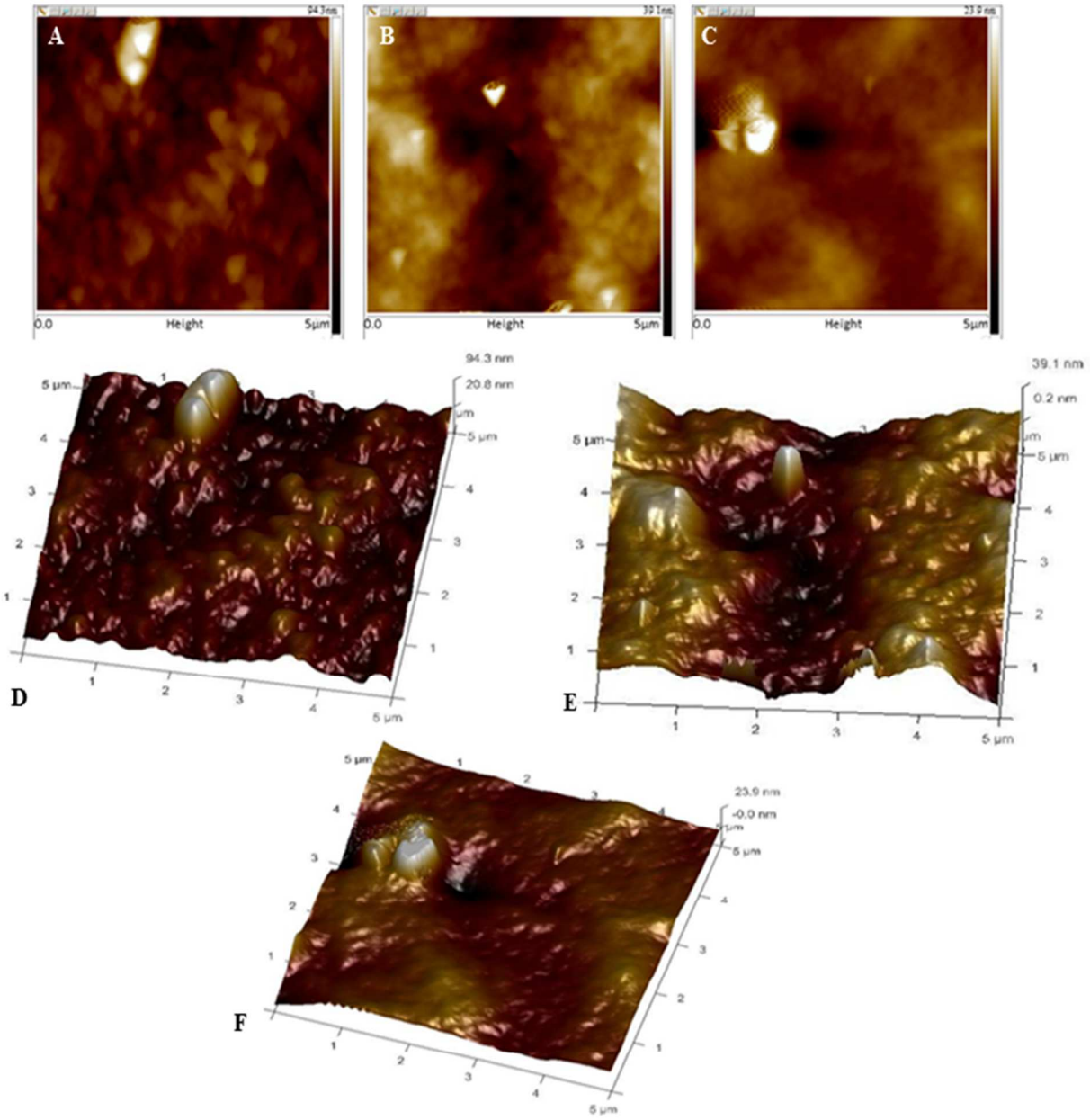

Fig. 7 Two-dimentional scans of A) S-0, B) S-1.0 and C) S-2.0 membranes and three dimensional scans of D) S-0, E) S-1.0 and F) S-2.0 membranes.

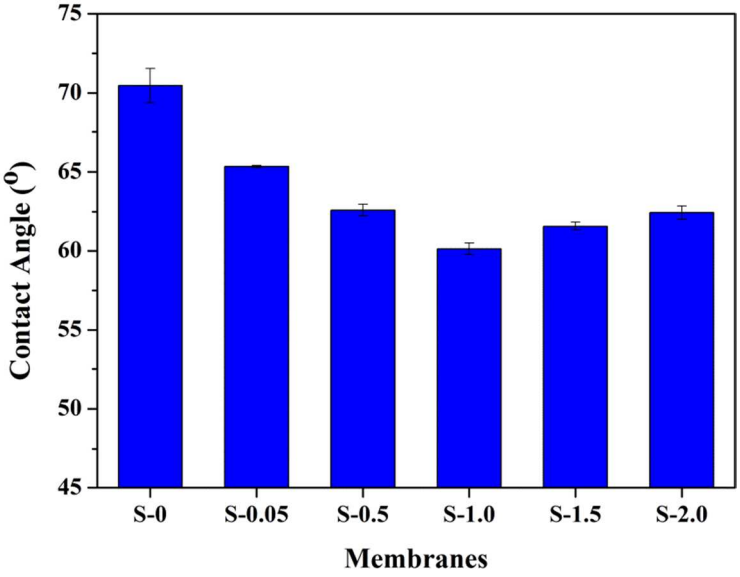

Fig. 8 Contact Angle of the membranes.

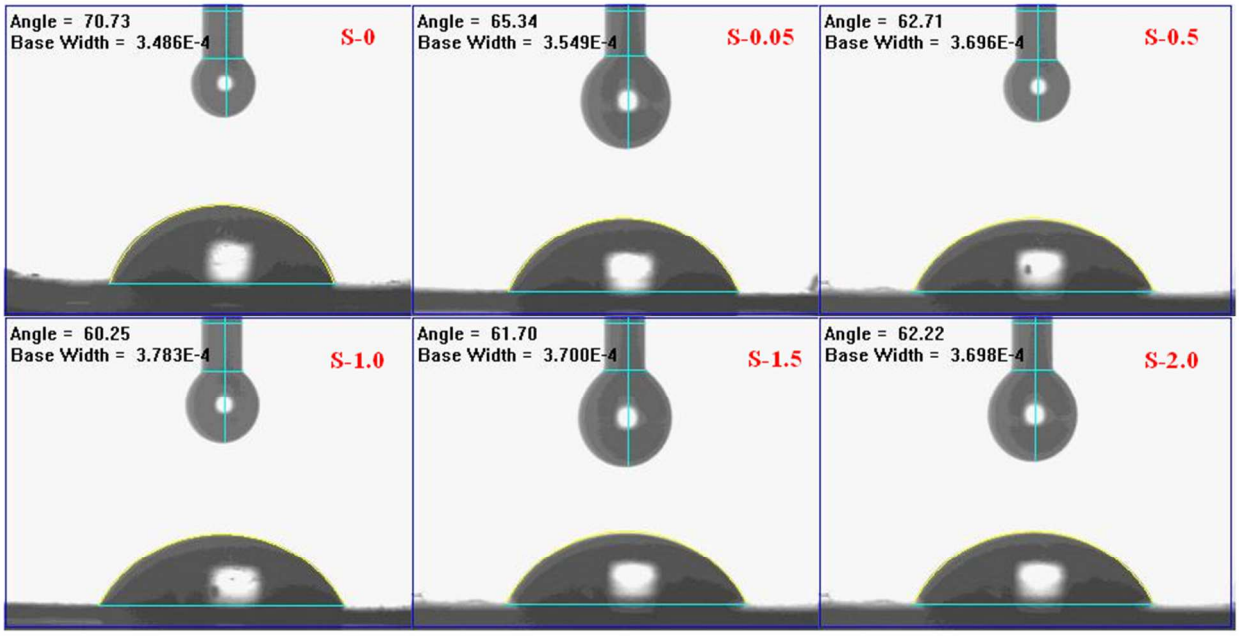

Fig. 9 Images of contact angles measured on membrane surfaces.

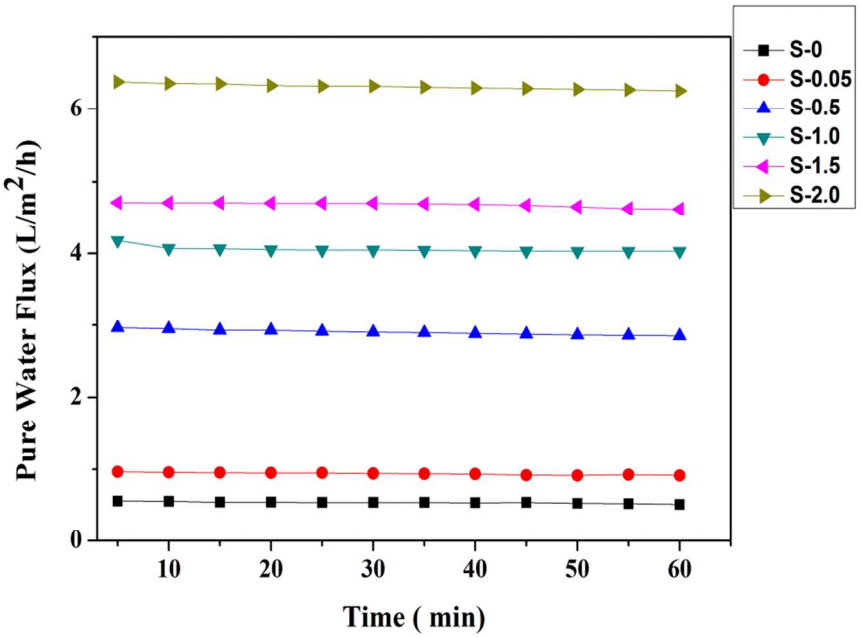

Fig. 10 Pure water flux of the membranes at 0.6 MPa .

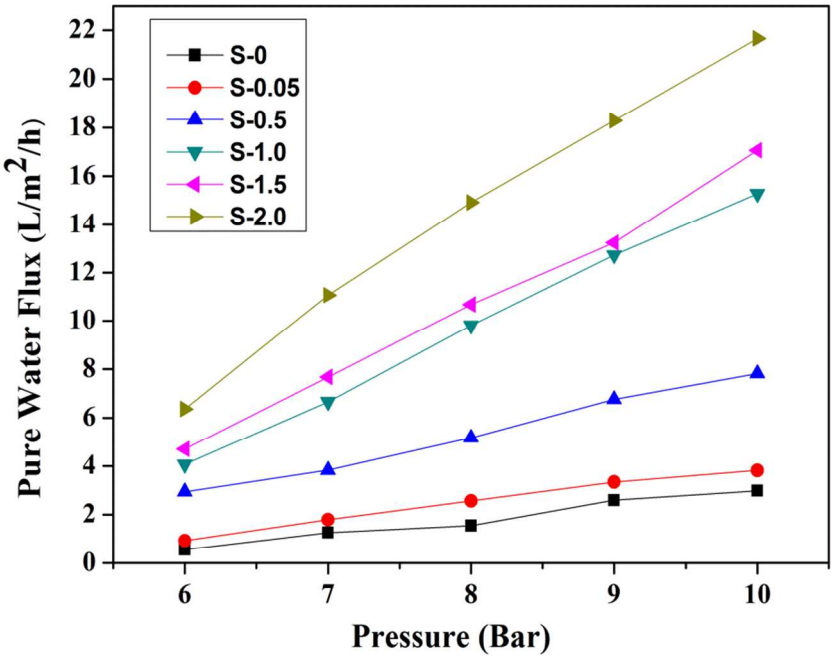

Fig. 11 Pure water flux vs. pressure.

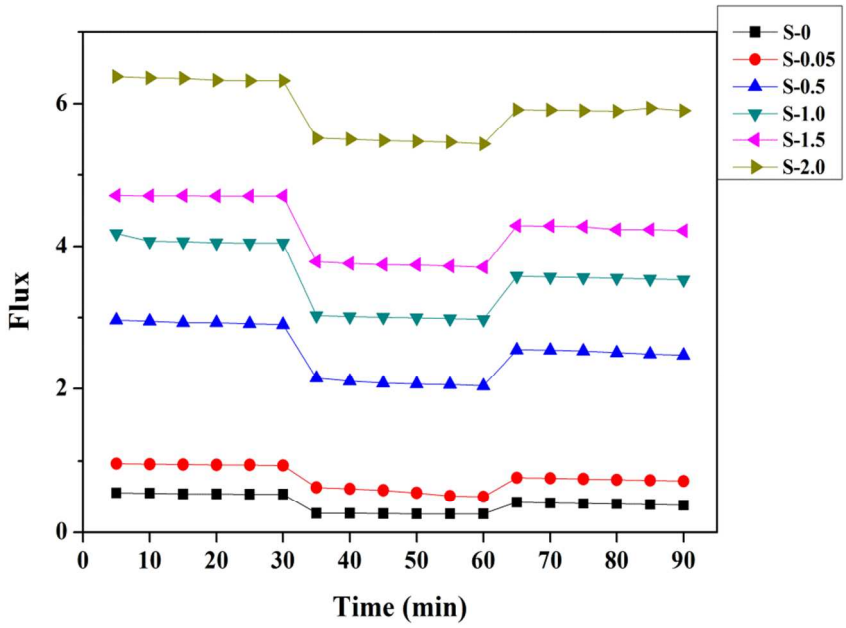

Fig. 12 Flux of the membranes during BSA filtration.

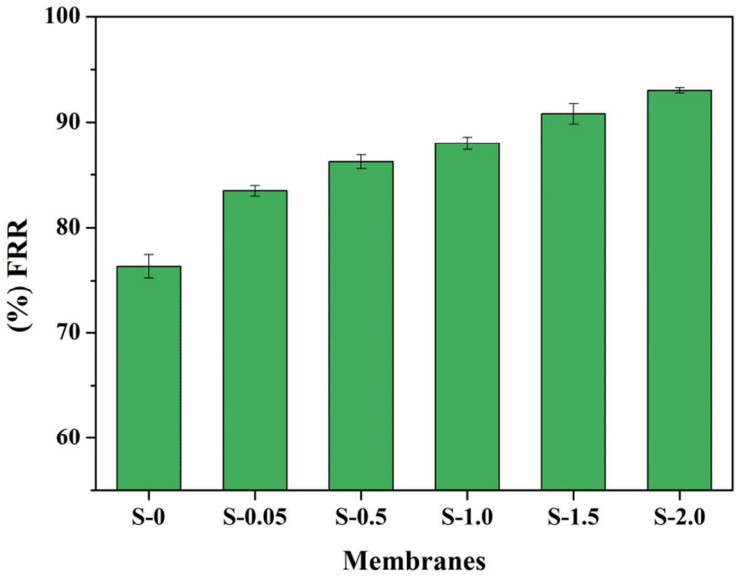

Fig. 13 Flux Recovery Ratio (FRR) of membranes.

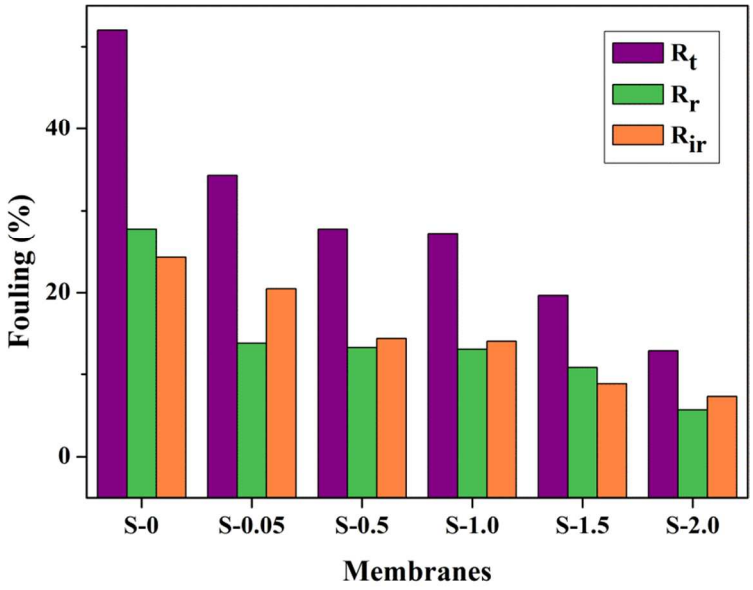

Fig. 14 Fouling of the membranes in terms of total total fouling (R_t), reversible fouling (R_r) and irreversible fouling (R_{ir})

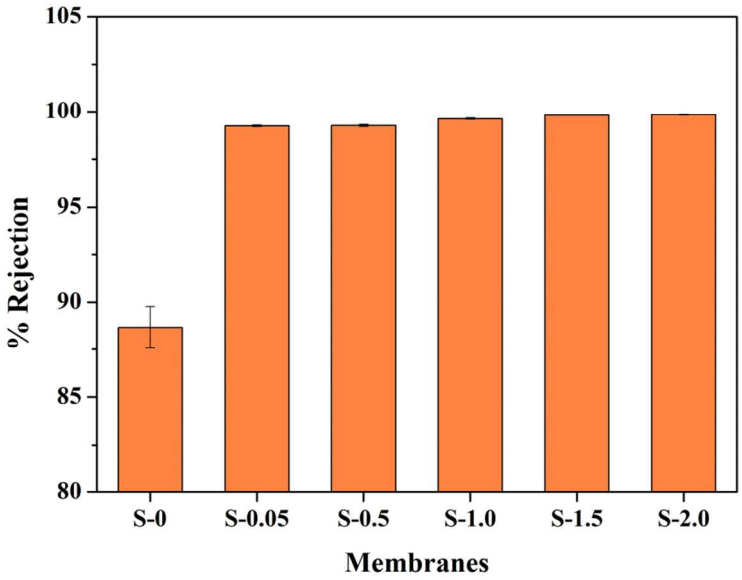

Fig. 15 BSA Rejection % by the membranes.

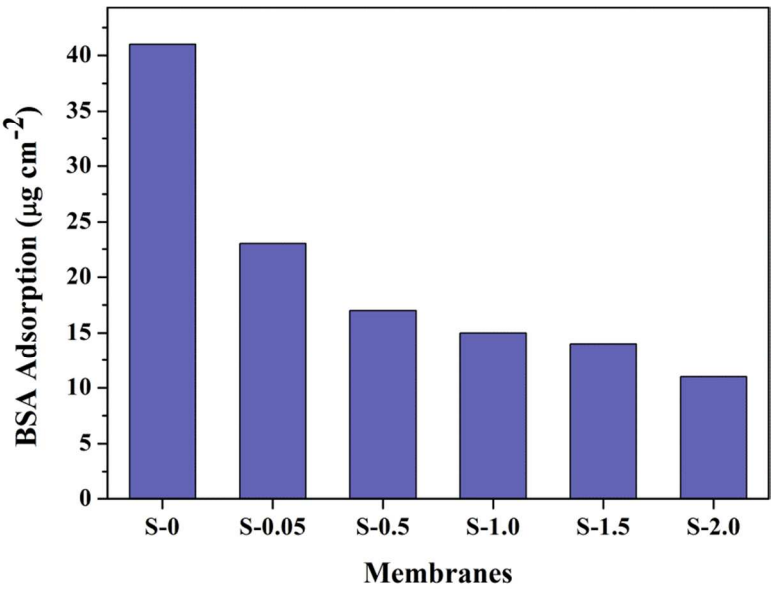

Fig. 16 BSA adsorption by membranes

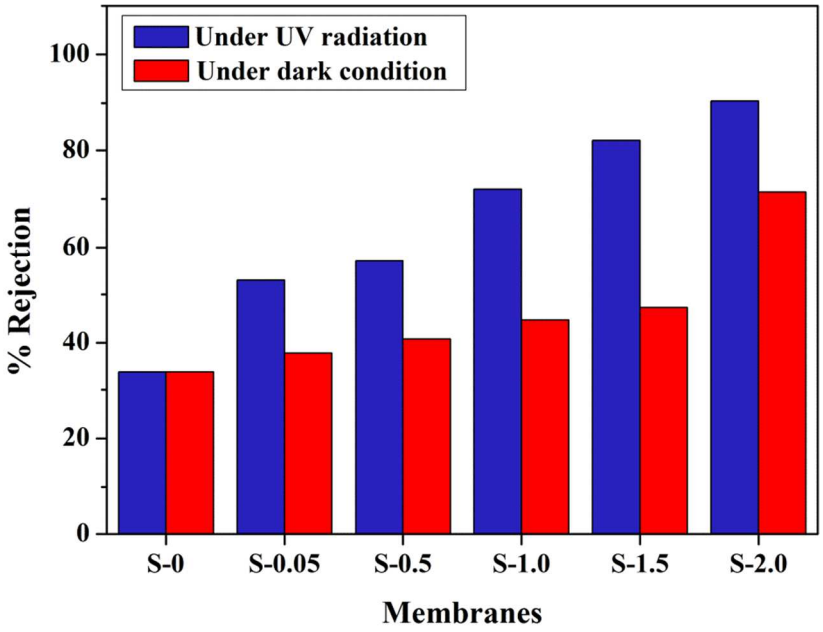

Fig. 17 MB dye rejection by the membranes at 10 ppm.

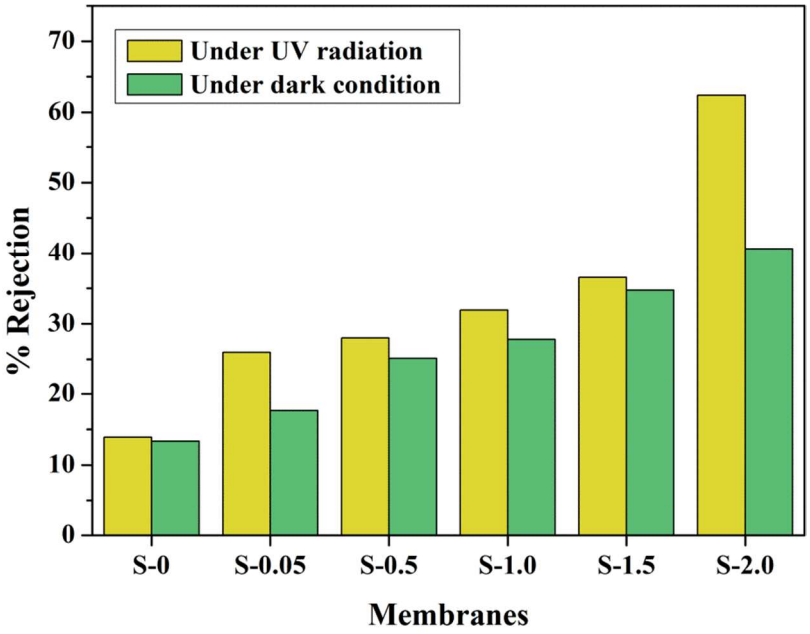

Fig. 18 MB dye rejection by the membranes at 20 ppm.

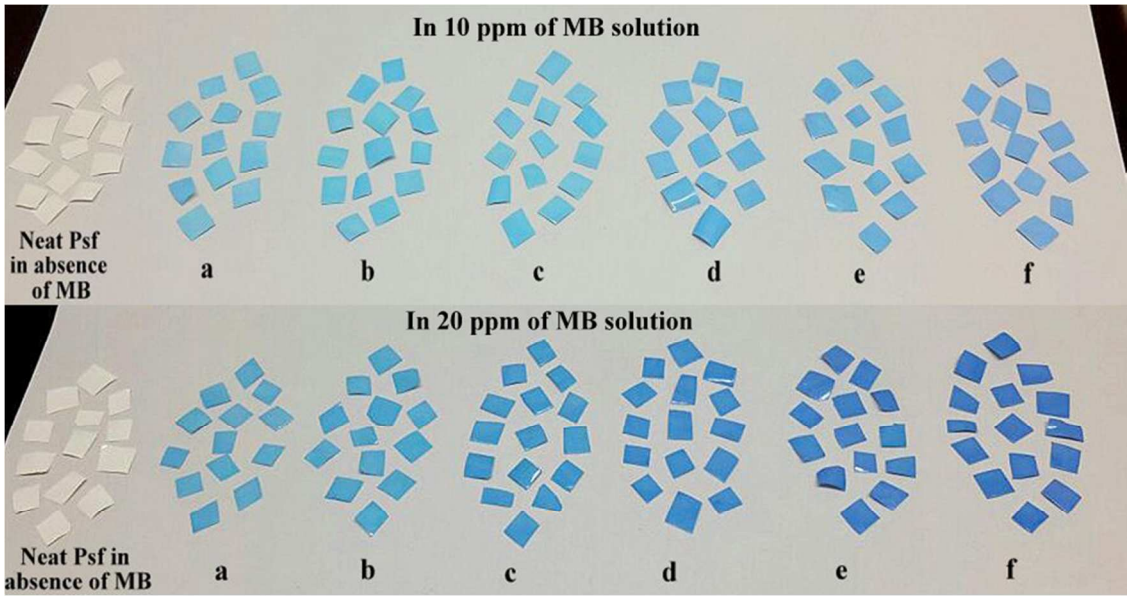

Fig. 19 The adsorption of MB on the membrane surface under dark conditions (a, b, c, d, e and f are membrane pieces of S-0, S-0.05, S-0.5, S-1.0, S-1.5 and S-2.0 respectively).

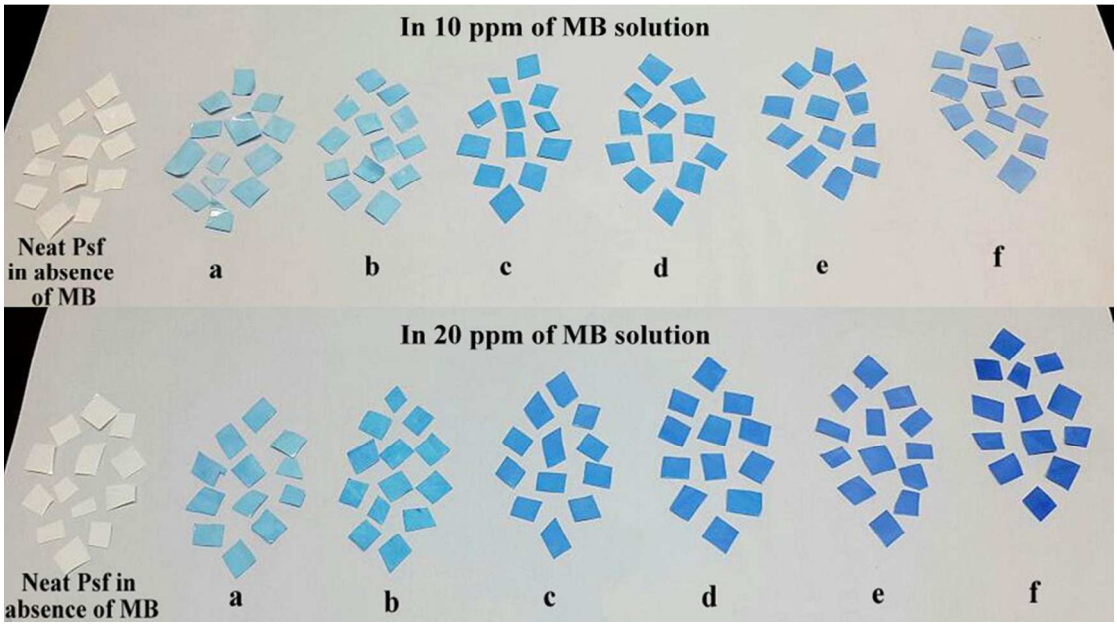

Fig. 20 The adsorption of MB on the membrane surface under UV (a, b, c, d, e and f are membrane pieces of S-0, S-0.05, S-0.5, S-1.0, S-1.5 and S-2.0 respectively).

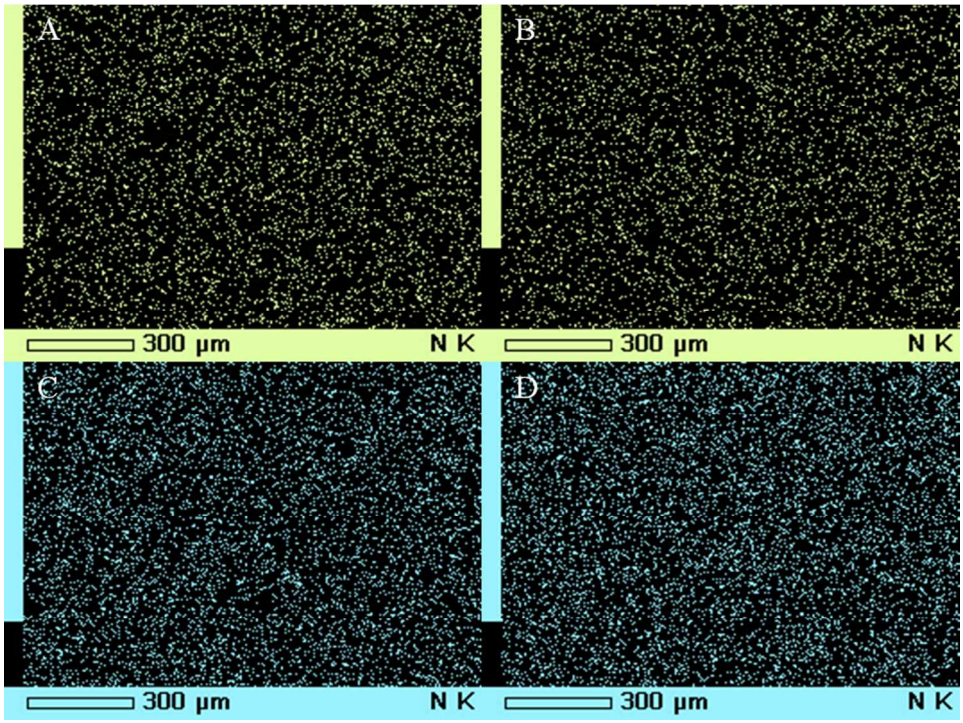

Fig. 21 Elemental mapping of N for adsorption of MB on the membrane surface (A, B are surfaces of S-0 membrane after adsorption at 10 ppm and C, D are the surfaces of S-2.0 membrane after adsorption at 20 ppm).

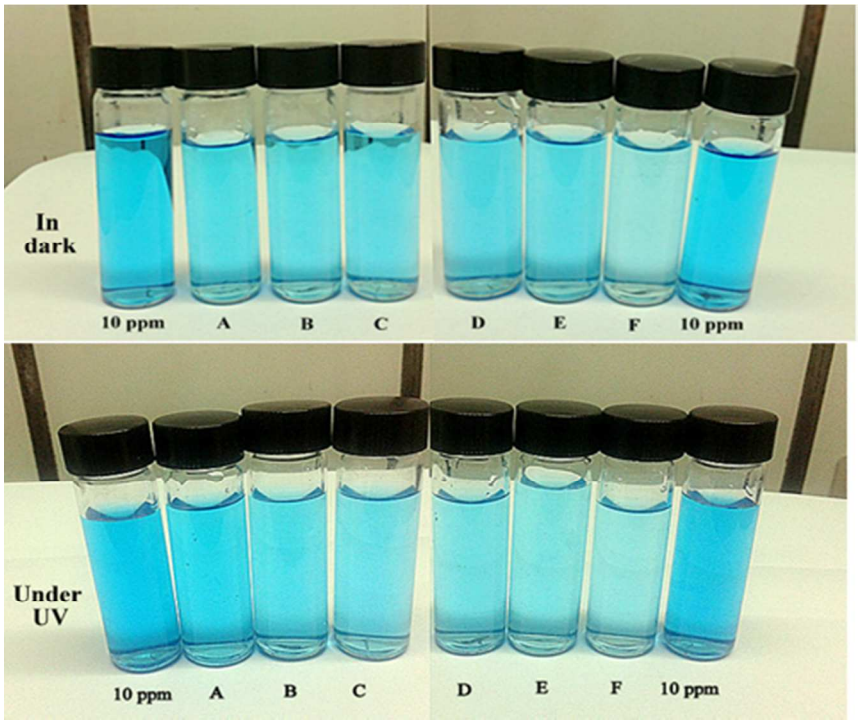

Fig. 22 Rejection of MB by membranes at 10 ppm (A, B, C, D, E and F are the solutions of MB after the rejection by the membranes S-0, S-0.05, S-0.5, S-1.0, S-1.5 and S-2.0 respectively).